PHYSICAL REVIEW E **68**, 055702(R) (2003)

Strouhal-Reynolds number relationship for bluff-body flows numerically simulated by an artificial boundary method

J. F. Ravoux,[1] M. Provansal,[1] A. Nadim,[2] and L. Schouveiler[1,*]
[1]*Institut de Recherche sur les Phénomènes Hors Equilibre, 49 rue F. Joliot Curie, Boîte Postale 146, 13384 Marseille Cedex 13, France*
[2]*Keck Graduate Institute and Claremont Graduate University, Claremont, California 91711, USA*
(Received 14 July 2003; published 20 November 2003)

The incidence of the numerical resolution and the blockage effect are investigated in an embedding method for solving bidimensional bluff body flows. This method consists of using an artificial boundary instead of imposing exact conditions on the body surface. It requires us to define a blur frontier ratio and a blockage effect ratio. The blockage effect ratio is found using the mean flow of a circular cylinder directly. The blur frontier ratio is obtained by comparison of the present method with another numerical method where explicit boundary conditions on the body are imposed. For this ratio, the investigations are based on the flow past a square cylinder which discard the uncertainty on the surface of the body for the embedding method. Hence, the two factors allow the transformations of the Strouhal and the Reynolds numbers for the flow past a circular cylinder. The universal Strouhal-Reynolds number relationship of the circular cylinder is finally recovered.

DOI: 10.1103/PhysRevE.68.055702 PACS number(s): 02.60.−x, 02.70.−c, 47.11.+j, 83.85.Pt

I. INTRODUCTION

The global dynamics of the flow past a circular cylinder is usually inferred through the following numbers: Reynolds $\mathrm{Re}=Ud/\nu$, Strouhal $\mathrm{St}=fd/U$, and Roshko $\mathrm{Ro}=\mathrm{Re}\times\mathrm{St}=fd^2/\nu$. They are based on the mean velocity at the cylinder U, its effective diameter d, the frequency of the vortex shedding f, the kinematic viscosity ν, and the density ρ of the fluid. A laminar vortex shedding regime is known to occur for the Reynolds number range extending approximately from 50 to 180 (see, e.g., Ref. [1]). Although the nominally parallel (bidimensional) shedding can be affected by three-dimensional phenomena giving rise to oblique vortices, there is now an agreement for the existence of a universal Strouhal-Reynolds number curve for the circular cylinder. The relationship is universal in the sense that the experimental and numerical data of the laminar vortex shedding collapse (within 1%) onto a single continuous curve for the parallel shedding as well as for oblique vortices when a geometric transformation is applied [2]. This makes the circular cylinder wake very suitable as a test flow for exploring various numerical methods such as the embedding method considered here. Details on the numerical treatment with such a method are given in Ref. [3]. In summary, calculations are effected on a Cartesian grid even for a circular, or more complex, geometry that thus allows the use of standard numerical routines. Moreover, the temporal discretization leads to a mainly explicit numerical scheme (except for the treatment of the pressure contribution), therefore it is simple to implement.

The input constant parameters in the numerical simulations are the inlet velocity U_∞ and the diameter of the cylinder d_∞, hence the Reynolds number Re_∞ is varied through the parameter ν. However, in real life experiments, the mean velocity U in the vicinity of the cylinder is the relevant value to quote the mechanisms of the dynamics of the wake. In consequence, the confinement effects need to be taken into account to accurately describe the actual flow observed in the numerical simulations. In addition, the embedding method approximates complex geometries of bluff-bodies using artificial frontiers [3]. It consequently creates a blur region at the cylinder's surface imposed by the mask function. Because a Cartesian grid is employed, the shape of a cylinder would have been perfectly rendered only for an infinite spatial resolution (or for a rectangular-shaped cylinder). Hence, in all simulations an effective diameter needs to be evaluated. These two corrections on the confinement and the blur frontier are required to compare accurately data issued from the numerical simulations and those from experiments.

II. SIMULATION DETAILS

The embedding method treats the two-dimensional hydrodynamics equations within a velocity-pressure formulation in their Eulerian form and on a regular Cartesian grid [3]. The lengths X and Y extend, respectively, in the longitudinal and transversal directions of the velocity components u and v. The temporal discretization is a forward differencing (first-order accuracy) involving three fractional steps in the time integration. The first step performs the integration of the advection and the diffusion terms in an explicit scheme. In the second step, a body force term is imposed in the momentum equation for the cells that are partially or fully occupied by the cylinder (using a mask function), the velocity field is modified so as to make it vanish in the cylinder. The third fractional step is the integration of the Poisson equation for pressure associated with the pressure gradient part of the momentum equation. The spatial discretization is based on central differencing (second-order accuracy) on a staggered grid for all the variables. In contrast to most numerical studies, boundary conditions on the cylinder are not set directly; rather they are satisfied implicitly at the second fractional

*Author to whom correspondence should be addressed. Electronic address: lionel.schouveiler@irphe.univ-mrs.fr

step. Concerning the velocity, the conditions on the lateral boundaries ($y=0$ and $y=Y$) are impermeability and free slip, the latter in order to avoid the formation of boundary layers on the lateral boundaries. At the outflow ($x=X$), the homogeneous Neumann conditions are applied in the longitudinal directions and uniform profile at the inflow ($x=0$). For the pressure, zero is imposed at the outlet, homogeneous Neumann conditions are applied at the inlet in the longitudinal direction and at the lateral walls in the transverse direction. The numerical parameters are deduced from the number of points needed to represent the dimensionless radius $d_\infty/2$ and the dimensionless time $d_\infty/2U_\infty$. They are, respectively, refered to as the grid spacing h and the time step τ; for the lower resolution, $h=0.2$ which implies 10 nodes for the diameter d_∞ as shown in Fig. 1. The data used further are produced at $h=0.2$, $h=0.1$ with $\tau=0.025$ concerning the flow past a square cylinder and at $h=0.2$, $h=0.1$ with $\tau=0.01$ concerning the flow past a circular cylinder. The critical Reynolds numbers of vortex shedding for the various numerical experiments are obtained by decreasing the Reynolds number from $\mathrm{Re}_\infty=55$ (where the flow is time-dependent) to different lower values and checking whether the wake oscillation is sustained. For the square cylinder flow, we obtain $44.75<\mathrm{Re}_\infty<45$ and $42.5<\mathrm{Re}_\infty<43$, whereas for the circular cylinder we obtain $50.5<\mathrm{Re}_\infty<50.75$ and $47<\mathrm{Re}_\infty<47.5$, provided the respective numerical parameters.

III. RESULTS

High resolution and large computational grid are generally adopted in simulations in order to meet ideal conditions of the flow discretization, which are computational time consuming. In this method, defining the actual size of the body and its distance from the lateral walls consist of the main corrections to apply to the data and optimize the accuracy and the computational load.

The corrections on the diameter and the velocity are taken into account via the correction factors: the blur frontier ratio $\beta=d/d_\infty$ and the blockage ratio $\alpha=U/U_\infty$. According to the definitions of the dimensionless parameters, they imply the following transformations between the experimental and the numerical dimensionless numbers:

$$\mathrm{Re}=\alpha\beta\,\mathrm{Re}_\infty,\quad \mathrm{Ro}=\alpha\beta\,\mathrm{Ro}_\infty,\quad \mathrm{St}=\mathrm{St}_\infty. \tag{1}$$

The first one is a consequence of uncertainty of the surface of the bluff body, inherent to the artificial boundaries methods, and the second is related to the well-known blockage effect.

Effective diameter. The sketch in Fig. 1 shows the nodes of the velocity components set on the staggered grid centered on the dashed lines grid where lengths are scaled on the grid spacing of the lower resolution ($h=0.2$). The longitudinal components are set on the right side of each cell (round symbols) and the transversal components at the top (square symbols), only the relevant nodes are represented in the figure. The perimeter of the cylinder that corresponds to the diameter d_∞ is assumed to follow the solid line and is centered on the cross, it is surrounded by an artificial solid/fluid transition (shaded in gray). The nodes where the velocity is let to zero for each time step consist of an artificial cylinder. It is located inside the transition region with the limiting nodes refered by round (u components) and square (v components) black symbols that form an approximate circular cylinder. Similarly, the nodes associated to unchanged velocity surround the transition region and form a perimeter that can be distinguished by the round and the square white symbols. The effective diameter is expected to be in the range between the two limiting artificial diameters associated to these two perimeters.

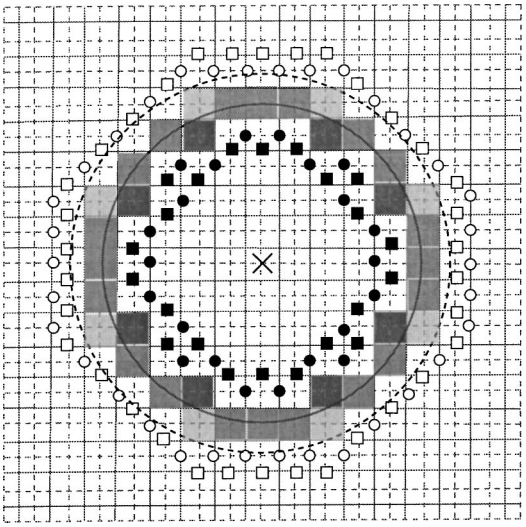

FIG. 1. Perimeters associated to diameters d ($-$), d_∞ ($--$) and transition region between body and fluid (shaded cells) on the stagered grid cell centered on the dashed grid, cylinder center ($\times$). Only the x components ($\bigcirc$) and y components ($\square$) limiting the transition region are represented.

It naturally follows that when the spatial resolution is increased dramatically, the core cylinder of zero velocity and the outer cylinder become true circles. They impinge the cylinder surface in a tiny region such that the cylinder can be assumed as circular. For the lower resolution ($h=0.2$), Fig. 1 shows that the effective perimeter associated to d lies approximately in the range $0.736\,d_\infty \leqslant d \leqslant 1.257\,d_\infty$. In other words, the effective diameter may be over or under estimated, and the inner and outer shapes differ from circles.

In order to determine the factor β, the numerical simulations are turned to the flow past a square cylinder which are performed at various spatial resolutions. For the embedding method, this particular geometry discards any uncertainty on the body shape. The inner cylinder of zero velocity and the outer cylinder are both true squares without approximation. Still there is an uncertainty on the size of the effective length d which is evaluated using β in the following. It is estimated as lying into the same range as for the circular cylinder case presented in Fig. 1. The Re-St relationship from the embedding method is compared to the relationship deduced from the data provided by Sohankar *et al.* [6]. They performed in particular two-dimensional numerical experiments of the flow past a square cylinder at zero incidence, that is when the side that faces the incoming flow is perpendicular to it. The

method used by these authors is an incompressible SIMPLEC code on a nonstaggered grid arrangement. A third-order QUICK scheme is used for the convective terms and an implicit time discretization with second order Crank-Nicholson scheme is employed. The Strouhal and Reynolds numbers are equally defined in both studies, the boundary conditions and the size of the grids are similar and in particular the blockage effect is the same with $Y=20\,d_\infty$. The time step is 0.025 and, for the study from Sohankar *et al.*, the spatial domain is mapped to get a grid spacing of 0.5 far from the body and of 0.004 at the body. Conversely, there is no mapping in the embedding method, that is the grid spacing is the same in all the spatial domain. We choose the resolutions $h=0.2$ and $h=0.1$ that are intermediate to this of Sohankar *et al.* It follows that the equivalence of the data obtained from the two alternate methods is ensured except for two points. The spatial resolutions differ in their principle of implementation, especially near the body, and the effective size of the body is fully determined in the study from Sohankar *et al.* whereas it is approximate in the embedding method. This latter feature allows to determine the effective diameter through $\beta=d/d_\infty$, assuming no other relevant difference between the two methods. Hence, any differences observed in the Re-St relationships would appear for different spatial resolutions in the embedding method, affecting the blur region and leading to the factor β.

The fit of the Reynolds-Strouhal numbers values provided by Sohankar *et al.* is written

$$\mathrm{St}_{ss}=A_{ss}+\frac{B_{ss}}{\mathrm{Re}_{ss}}+C_{ss}\,\mathrm{Re}_{ss} \tag{2}$$

with $A_{ss}=0.187823$, $B_{ss}=63.8306$, and $C_{ss}=-8.243243\times10^{-6}$ for $\mathrm{Re}_{ss}=\{55,60,100,150,200\}$. The functional form (2) used for the St(Re) fit results from Landau-type models commonly used to describe the dynamics of the shedding modes (see, e.g., Ref. [4]). A similar form was also deduced by Rayleigh [5] from a series expansion of the shedding frequency in terms of Re^{-1} considered as a small parameter.

The introduction of the ratio β on values of Strouhal and Reynolds numbers obtained from the embedding method leads to the following formula:

$$\mathrm{St}_\infty=A_{ss}+\frac{B_{ss}}{\beta\,\mathrm{Re}_\infty}+\beta C_{ss}\,\mathrm{Re}_\infty\,. \tag{3}$$

The ratio β is determined by nonlinear curve fitting for $\mathrm{Re}_\infty=\{55,60,65,70,75,80,85,100\}$ and subsequent values of St_∞ obtained for the two spatial resolutions. These specific values of Reynolds numbers are chosen where the time-dependent wake is laminar in a range where the mean vortex shedding flow is laminar. For the time step $\tau=0.025$, we obtain $\beta=1.2032$ when $h=0.2$ and $\beta=1.1701$ when $h=0.1$. Transposed to the case of the circular cylinder, the uncertainty on the blur region remains the same because it is not based on the shape of the body but on the grid spacing, hence for each grid the corresponding value of β is used. Figure 1 shows the effective perimeter in dashed line associated to the calculated value of β for $h=0.2$. Hence, we observe that the diameter d_∞ underestimates the diameter of the cylinder.

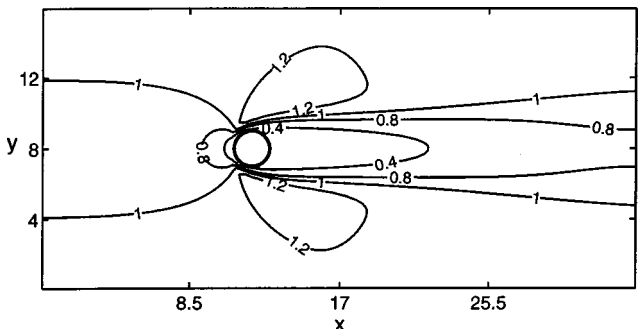

FIG. 2. Longitudinal velocity field Vx of mean flow for $\mathrm{Re}_\infty=55$ for the circular cylinder.

Blockage effect. Free slip boundary conditions are imposed on lateral walls for the sake of conserving the condition of parallel and uniform flow present at the inlet. This tries to reproduce an experimental setup with far away walls to allow a constant velocity profile everywhere reasonably far from the body. Nevertheless, the condition of the conservation of the flow rate involves an increase of the longitudinal velocity in the region near the cylinder. The effect is shown in Fig. 2 for the spatial domain with size $X=17\,d_\infty$ and $Y=8\,d_\infty$ (here presented in units of the cylinder radius $d_\infty/2$) for the mean longitudinal flow field over one period of the stationary vortex shedding. The flow accelerates strongly in the cylinder region between the two walls. The longitudinal velocity profiles in Fig. 3 show the increase in the x direction near the walls with approximately zero derivative in the y direction. Notice that the velocity is zero with a length corresponding to the diameter for the profile that passes through the cylinder center (solid line) at the location $x=X_0$. The velocity used as reference in the dimensionless numbers is taken on this profile in most experimental studies.

The blockage ratio correction $\alpha=U/U_\infty$ refers to U at the walls for the profile at the x location $x=X_0$. The effective velocity U is deduced directly from the values of Vx on the walls as presented in Fig. 3. This figure suggests that the velocity in the x direction remains unchanged in the y direction, here we deduce $\alpha=1.1353$ ($h=0.2$, $\tau=0.01$) and $\alpha=1.1333$ ($h=0.1$, $\tau=0.01$). Notice the weak difference between these two ratios although the spatial resolutions are of factor 2, similar remark applies when other temporal resolutions are used.

Correction of the Re-St relationship. Figure 4 shows the five values for the flow past a square cylinder from Sohankar *et al.* [+: data, $--$: formula (2)] and data from Owen [7] ($\times$). Owen performed an experimental study and the related data show the occurrence of 3D effects near $\mathrm{Re}=170$ as a discontinuity. The proximity of the two sets validates that the square cylinder is equally well reproduced in these two studies. Concerning the embedding method, the data directly extracted from the numerical simulations correspond to $h=0.2$ ($\square$), $h=0.1$ ($\diamond$) for $\tau=0.025$. The value of β at the respective numerical resolutions is determined such that the data associated to the two studies match, according to Eq.

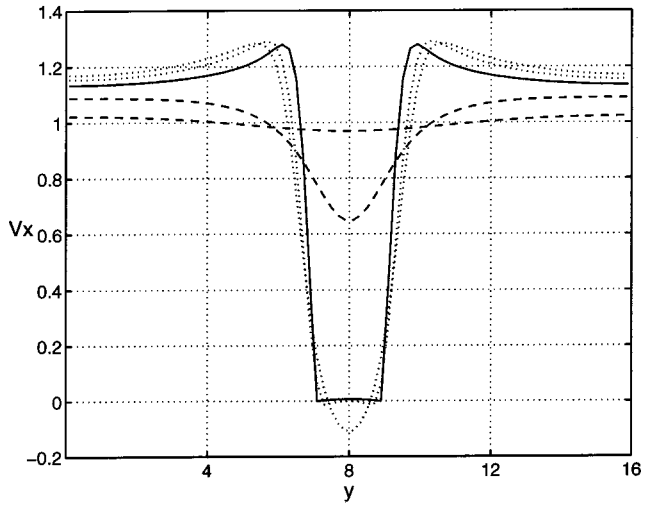

FIG. 3. Longitudinal velocity profiles of mean flow for $Re_\infty = 55$ and transverse length in units of the cylinder's radius. The profiles are consecutive with Vx between 1 and 1.2 where $y=16$ and are located at the longitudinal distances from the center of the cylinder $-3d$, $-d$ (dashed), 0 (solid), and $d/2$ and d (dotted).

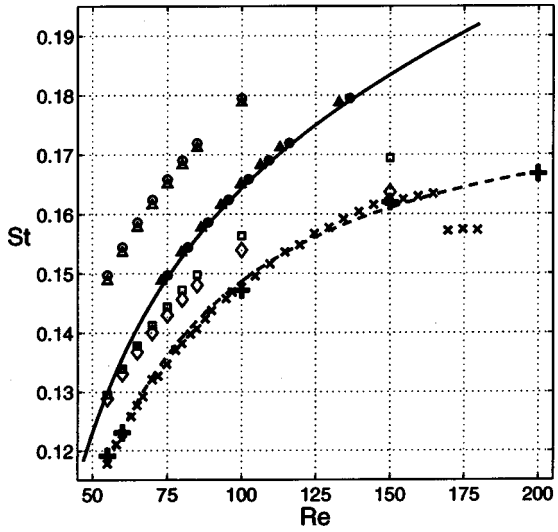

FIG. 4. Strouhal number as function of the Reynolds number. Square cylinder: Sohankar *et al.* data: +, fitted curve: $--$; Owen: $\times$; embedding method ($\tau=0.025$), raw data $h=0.2$: $\square$ and $h=0.1$: $\diamond$. Circular cylinder: universal curve from Williamson [2], $-$; Embedding method ($\tau=0.01$) $h=0.2$: $\bigcirc$,$\bullet$; and $h=0.1$: $\triangle$,$\blacktriangle$ (raw data: $\bigcirc$, $\triangle$ and corrected values: $\bullet$,$\blacktriangle$).

(3). Concerning the flow past a circular cylinder, the universal curve given by Williamson [2] (solid line) is above the curves obtained for the cases of a square cylinder.

The data obtained from the embedding method at $\tau=0.01$, $h=0.2$, and $h=0.1$ when no correction is applied ($\bigcirc$,$\triangle$) lie in the upper left corner. When transformed via the equations in Eq. (1) using the appropriate factors associated to the specific resolutions, the values ($\bullet$,$\blacktriangle$) meet the curve from Williamson. Provided that the agreement between all experimental results reported in literature agree into a 2% margin about this universal curve, the final values obtained by the Embedding Method lie into the expected limits.

IV. CONCLUSIONS

This study shows that the universal Re-St curve from Williamson [2] has been recovered with accuracy regardless to the numerical resolution of the embedding method. It is based on the independent determination of the blockage ratio α and the blur region ratio β. The first one is deduced directly from the generated data. The second one is obtained by comparison of the present numerical simulations with a reference study from Sohankar *et al.* concerning the flow past a square cylinder. Combining these two investigations, the dimensionless Strouhal and Reynolds numbers are deduced from the transformations where both factors are used according to appropriate numerical resolutions. Agreement of the resulting data with those from Williamson points out that the approximate size of the body is a key feature of the embedding method. It is the origin of the bias observed between Re-St relationships issued from this method and any other study. Hence, this bias can be resolved supported by arguments presented in this study. Furthermore, although these results are relevant for a two-dimensional geometry, such effects exist for applications and real cases as well. In consequence, a similar methodology can be used to treat general three-dimensional flows.

[1] C. H. K. Williamson, Annu. Rev. Fluid Mech. **28**, 477 (1996).
[2] C. H. K. Williamson, Phys. Fluids **31**, 2742 (1988).
[3] J. F. Ravoux, A. Nadim, and H. Haj-Hariri, Int. J. Comput. Fluid Dyn. **16**, 1 (2003).
[4] C. Mathis, M. Provansal, and L. Boyer, J. Phys. (France) Lett. **45**, L483 (1984).
[5] Lord Rayleigh, *The Theory of Sound*, 2nd ed. (MacMillan, London, 1896).
[6] A. Sohankar, C. Norberg, and L. Davidson, Int. J. Numer. Methods Fluids **26**, 39 (1998).
[7] J. C. Owen, Ph.D. thesis, University of London, 2000.